Precision Engineering 42 (2015) 133–142

Contents lists available at ScienceDirect

Precision Engineering

journal homepage: www.elsevier.com/locate/precision

Multivariate control charts for monitoring internal camera parameters in digital photogrammetry for LSDM (Large-Scale Dimensional Metrology) applications

Fiorenzo Franceschini*, Maurizio Galetto, Gianfranco Genta

Politecnico di Torino, DIGEP—Department of Management and Production Engineering, Corso Duca degli Abruzzi 24, 10129 Torino, Italy

ARTICLE INFO

Article history:
Received 7 November 2014
Received in revised form 26 March 2015
Accepted 17 April 2015
Available online 24 April 2015

Keywords:
Photogrammetry
Large-Scale Dimensional Metrology (LSDM)
Calibration process
Camera parameters
System diagnostics
Multivariate control chart

ABSTRACT

Industrial non-contact dimensional measurements using photogrammetry rely critically upon stability in time of camera calibration. This is particularly relevant for multi-camera systems employed for continuous and/or long term monitoring of some dimensional process, e.g. dimensional checks of the same manufactured component as it comes off the production line. In most of these cases, camera calibration is updated regularly to ensure optimal accuracy. Specifically, the use of photogrammetric systems requires the knowledge of both internal and external camera parameters estimated by calibration. Constancy of both sets is required during use. Internal parameters, pertaining to camera-specific properties, require stability over the operational lifespan of the system, while external parameters, concerning location and orientation, may change between calibrations. A diagnostic method for internal parameters based on multivariate control charts is proposed. The purpose of this method is to provide a comprehensive stability control over all the performed calibrations, especially for those systems used for regular monitoring of production lines. By integrating chart building into calibration software, no additional steps are added to the operator's workload for the calibration process. A practical application of the described methodology is presented at the end of the paper.

1. Introduction

Use of optical methods for dimensional measurements in industry is becoming widespread, with photogrammetry playing a key role in Large-Scale Dimensional Metrology [5,34,32,7,1,24,31,42]. Applications range from monitoring of buildings and monuments to control of large mechanical components such as aircraft wings and fuselages, ship hulls, etc.; they concern both occasional dimensional checks of finished products and for regular monitoring on production lines [44,29,10,37,21].

Multi-camera photogrammetric systems may be positioned around the object of interest, within an extensive measurement space where monitoring of dynamic objects is also possible. Change of measurement configuration entails a new calibration; this step represents a critical point for the use of the system [25,22,9].

Calibration produces the values for external and internal parameters given the operational constraints [25,22]. External parameters describe the spatial configuration of the system, i.e. position and orientation of the cameras in the measurement space. These parameters change whenever cameras are moved. On the other hand, internal parameters describe the technical characteristics of the cameras. These parameters change when camera-specific elements are altered, such as lenses or settings, or if drift/damage occurs. Several different procedures for calibration are described in literature, e.g. based on the use of calibrated artefacts, implementation of specific procedures, or a combination of both [8,46,25,39,22,7,3].

For those situations that require a continuous and/or long-term monitoring of some dimensional process, such as production lines, calibration parameters are updated regularly in order to ensure optimal performance. In these cases, current approaches incorporate calibration into the measurement process with no additional hardware effort. These procedures may guarantee reliable and accurate results, limiting the regular use of external artefacts. See, for example, commercial photogrammetric systems Quality Gate by Mapvision or TubeInspect by Aicon [1,24].

The correctness of calibration may be checked using reference artefacts, a proven, reliable approach, the implementation of which may, however, be difficult, expensive and time consuming [25,22]. An alternative approach may be based on the monitoring of internal parameters after each calibration, thereby relying on control

* Corresponding author. Tel.: +39 0905647225.
E-mail address: fiorenzo.franceschini@polito.it (F. Franceschini).

http://dx.doi.org/10.1016/j.precisioneng.2015.04.008
0141-6359/

of the stability (VIM 4.19 [16]) of camera parameters in order to check correctness of calibration. Unless otherwise stated, the term stability used in this document refers specifically to the VIM definition. The alternative approach is particularly helpful and effective for those photogrammetric systems used in production lines, for which calibration is performed frequently at regular time intervals.

Despite the problem of testing camera internal parameters, stability is a topic widely investigated in the scientific literature, and its solution remains the subject of ongoing investigation within the photogrammetric community [19]. Most approaches are based on the use of reference artefacts or simulation methods [18,4,11,12,36,43].

The use of multivariate control charts for monitoring internal parameter stability is proposed in this paper. In general, multivariate control charts are used whenever simultaneous control of two or more quality characteristics is required [15,27]. The proposed approach applies multivariate control charts as diagnostic tools for evaluating the stability of internal parameters after each calibration; calibration results are directly used for the diagnosis. The procedure may be automated by embedding the relevant routines in calibration software, without requiring any additional operation.

After each calibration a check is performed on measured values of the internal parameters using a specific multivariate control chart. Hence, troubles, such as faulty calibration procedure or camera damage/drift, which produce significant variations of internal parameters, will be detected and deemed *out-of-control* in the control chart, thereby requiring specific investigation.

The proposed approach covers:

(i) definition of internal parameters to be monitored;
(ii) construction of control chart;
(iii) acquisition of calibration data and implementation of calibration algorithm;
(iv) verification via control charts whether the set of internal parameters is acceptable (no *out-of-control* data);
(v) otherwise, causes are identified and remedial action is taken.

A short description of the basic principles of photogrammetry follows, introducing equations relating external and internal parameters to point location. The concepts of multivariate control charts are described along with their associated theoretical justification. A practical application to a real multi-camera system is then presented in order to show the potentialities of the method.

2. Basics of photogrammetry

Photogrammetry typically uses a distributed network of cameras, properly placed within the measurement volume in order to estimate 3D coordinates of one or more optical markers (or visually discernible features) positioned in the "field-of-view" of every camera (see Fig. 1). Generally, data processing is performed by an external DPU (Data Processing Unit), which is connected either wirelessly or by cable.

The 3D coordinates of a certain optical marker M_j can be related to the 2D coordinates of the corresponding image point $P_{i,j}$ in the i-th camera projection plane in terms of camera technical parameters, position and orientation, through the *collinearity equations* using homogenous coordinates (see Fig. 2) [25,22]:

$$\lambda_i \times \begin{bmatrix} u_{i,j} \\ v_{i,j} \\ 1 \end{bmatrix} = \boldsymbol{K}_i \times \boldsymbol{W}_i \times \begin{bmatrix} x_{M_j} \\ y_{M_j} \\ z_{M_j} \\ 1 \end{bmatrix} = \boldsymbol{P}_i \times \begin{bmatrix} x_{M_j} \\ y_{M_j} \\ z_{M_j} \\ 1 \end{bmatrix} \quad (1)$$

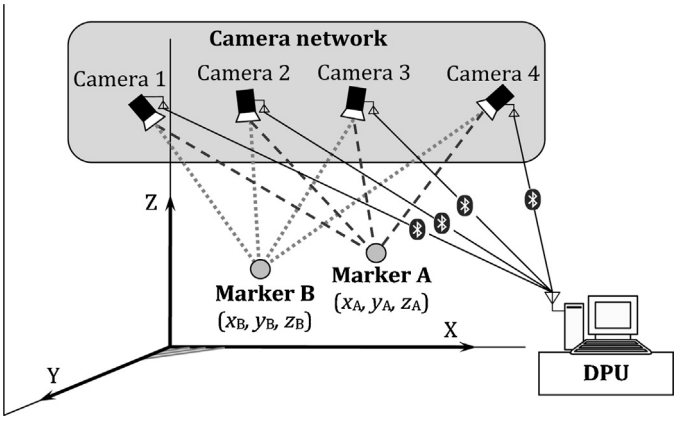

Fig. 1. Example of camera network configuration in a photogrammetric system with DPU bluetooth connection [7].

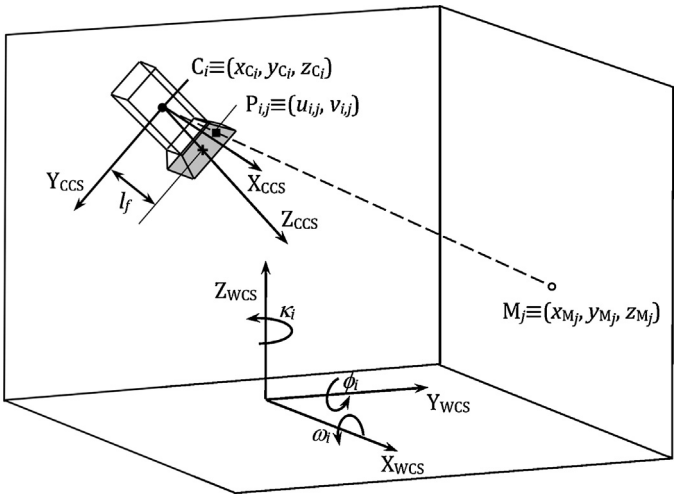

Fig. 2. Setup of a generic, camera-based localization problem in 3D space (adapted from [7], with permission).

where λ_i is a nonzero scale factor, $\boldsymbol{K}_i \in \mathbb{R}^{3,4}$ is the matrix of internal parameters (i.e. the two coordinates of the image center u_{0_i} and v_{0_i}, and the camera-related components u_{f_i} and v_{f_i} of the focal length l_f in the camera view plane), defined as:

$$\boldsymbol{K}_i = \begin{bmatrix} u_{f_i} & 0 & u_{0_i} & 0 \\ 0 & v_{f_i} & v_{0_i} & 0 \\ 0 & 0 & 1 & 0 \end{bmatrix} \quad (2)$$

$\boldsymbol{W}_i \in \mathbb{R}^{4,4}$ is the matrix of external parameters (i.e. the camera projection center coordinates x_{C_i}, y_{C_i} and z_{C_i}, and the camera orientation angles ω_i, ϕ_i, and κ_i), defined as:

$$\boldsymbol{W}_i = \begin{bmatrix} & & & -x'_{C_i} \\ & \boldsymbol{R}_i & & -y'_{C_i} \\ & & & -Z'_{C_i} \\ 0 & 0 & 0 & 1 \end{bmatrix} \quad (3)$$

where $(x'_{C_i}, y'_{C_i}, z'_{C_i})$ are the coordinates of the projection center C_i in the local camera reference frame F_{CCS}, and $\boldsymbol{R}_i \in \mathbb{R}^{3,3}$ is the rotation

matrix, which relates the world coordinate reference frame F_{WCS} and the local camera reference frame F_{CCS}:

$$\boldsymbol{R}_i = \begin{bmatrix} \cos(\kappa_i)\times\cos(\phi_i) & \cos(\kappa_i)\times\sin(\phi_i)\times\sin(\omega_i)-\sin(\kappa_i)\times\cos(\omega_i) & \cos(\kappa_i)\times\sin(\phi_i)\times\cos(\omega_i)+\sin(\kappa_i)\times\sin(\omega_i) \\ \sin(\kappa_i)\times\cos(\phi_i) & \sin(\kappa_i)\times\sin(\phi_i)\times\sin(\omega_i)+\cos(\kappa_i)\times\cos(\omega_i) & \sin(\kappa_i)\times\sin(\phi_i)\times\cos(\omega_i)-\cos(\kappa_i)\times\sin(\omega_i) \\ -\sin(\phi_i) & \cos(\phi_i)\times\sin(\omega_i) & \cos(\phi_i)\times\cos(\omega_i) \end{bmatrix} \quad (4)$$

The matrix $\boldsymbol{P}_i \in \mathbb{R}^{3,4}$, obtained from (1), is called camera projection matrix.

The ideal model described in Eq. (1) provides only an approximation because imaging errors are liable to substantially affect the accuracy of localization of optical markers. Corrections are applied to the image coordinates in order to reduce lens distortion errors as much as possible. Radial, tangential, and skewness distortion have been identified by previous authors as being the primary types of imaging errors [25,22].

These error components are usually evaluated using polynomial models, the coefficients of which are denoted as distortion coefficients. The total lens distortion correction, as introduced in the collinearity equations, can be expressed as [25,22]:

$$\begin{bmatrix} \tilde{u}_{i,j} \\ \tilde{v}_{i,j} \\ 1 \end{bmatrix} = \begin{bmatrix} 1 & 0 & \delta u_{R_{i,j}} + \delta u_{T_{i,j}} + \delta u_{S_{i,j}} \\ 0 & 1 & \delta v_{R_{i,j}} + \delta v_{T_{i,j}} \\ 0 & 0 & 1 \end{bmatrix} \begin{bmatrix} u_{i,j} \\ v_{i,j} \\ 1 \end{bmatrix} \quad (5)$$

where $\delta u_{R_{i,j}}$ and $\delta v_{R_{i,j}}$ represent the radial distortion:

$$\begin{aligned} \delta u_{R_{i,j}} &= \left[k_{C1_i} \times \left(u_{i,j}^2 + v_{i,j}^2\right) + k_{C2_i} \times \left(u_{i,j}^2 + v_{i,j}^2\right)^2 + k_{C5_i} \times \left(u_{i,j}^2 + v_{i,j}^2\right)^3 \right] u_{i,j} \\ \delta v_{R_{i,j}} &= \left[k_{C1_i} \times \left(u_{i,j}^2 + v_{i,j}^2\right) + k_{C2_i} \times \left(u_{i,j}^2 + v_{i,j}^2\right)^2 + k_{C5_i} \times \left(u_{i,j}^2 + v_{i,j}^2\right)^3 \right] v_{i,j} \end{aligned} \quad (6)$$

$\delta u_{T_{i,j}}$ and $\delta v_{T_{i,j}}$ are the components related to the tangential distortion:

$$\begin{aligned} \delta u_{T_{i,j}} &= 2 \times k_{C3_i} \times u_{i,j} \times v_{i,j} + k_{C4_i} \times \left(3 \times u_{i,j}^2 + v_{i,j}^2\right) \\ \delta v_{T_{i,j}} &= 2 \times k_{C4_i} \times u_{i,j} \times v_{i,j} + k_{C3_i} \times \left(u_{i,j}^2 + 3 \times v_{i,j}^2\right) \end{aligned} \quad (7)$$

and $\delta u_{S_{i,j}}$ is related to the skewness distortion:

$$\delta u_{S_{i,j}} = \alpha_i \times v_{i,j} \quad (8)$$

Localization consists of determining the 3D coordinates of a marker M_j from its 2D image coordinates from several cameras. According to Eqs. (1) and (4), in the case that only one camera view is available, only the direction to the point M_j can be determined. Therefore, complete localization entails observing the point marker from at least two different camera positions. The identification of marker coordinates is achieved by finding the intersection of two or more direction vectors. The general rule is three points of overlap: two as the minimum requirement and one for redundancy. The localization procedure then follows according to fundamentals of digital photogrammetry [25,22].

3. Estimation of camera parameters

According to Section 2, each camera is characterized by a set of internal parameters $(u_{0_i}, v_{0_i}, u_{f_i}, v_{f_i})$, which represents its technical features, a set of correction parameters $(k_{C1_i}, k_{C2_i}, k_{C3_i}, k_{C4_i}, k_{C5_i}, \alpha_i)$ related to distortion effects, and a set of external parameters $(x_{C_i}, y_{C_i}, z_{C_i}, \omega_i, \phi_i, \kappa_i)$, pertaining to position and orientation with respect to a coordinate reference frame. Hence, network calibration consists of defining these 16 parameters for each camera of the system.

The multi-camera calibration problem is generally approached using a fully-automatic single-point self-calibration technique [39,31,42], requiring at least three cameras and a reference artefact for aligning and scaling the reference system. A single reflective marker, placed in several randomly-selected positions within the working volume, is tracked by the cameras. Image acquisition and processing provide pixel coordinates in the camera view plane corresponding to different optical marker positions (see Fig. 3).

The calibration algorithm performs a preliminary procedure aimed at discarding outliers [2], due to parasitic reflections in the working environment or measurement errors of the tracking engine. False points are removed from the list of visible points of the cameras according to an iterative pairwise analysis and a 2D reprojection error-based strategy [39]. Point-to-point correspondence is analyzed according to epipolar geometry constraints [13] and applying a RANSAC (RANdom SAmple Consensus)-based technique [6] for discarding outliers.

After outlier filtering, the calibration algorithm implements an iterative procedure to compute the projective structure (i.e. the projection matrix in Eq. (1) and the re-constructed cloud of 3D points) and estimate the correction parameters for camera lens distortion, also known as the lens distortion model [39]. Since external camera parameters are provided in a conventional reference frame, with conventional origin and scale, a further step for aligning and scaling the coordinate system is performed. For this step, a calibrated *scale-bar* is typically used as reference artefact [7].

In particular, the goal of the calibration is to estimate for each camera the scale parameter λ_i and the projection matrix $\boldsymbol{P}_i$ (see Eq. (1)).

According to Svoboda's approach [39], given n points (marker positions) and m cameras, the estimates can be obtained starting from the following expression:

$$\boldsymbol{Q} = \begin{bmatrix} \lambda_1 \times \begin{bmatrix} u_{1,1} \\ v_{1,1} \\ 1 \end{bmatrix} & \cdots & \lambda_1 \times \begin{bmatrix} u_{1,n} \\ v_{1,n} \\ 1 \end{bmatrix} \\ \vdots & \vdots & \vdots \\ \lambda_m \times \begin{bmatrix} u_{m,1} \\ v_{m,1} \\ 1 \end{bmatrix} & \cdots & \lambda_m \times \begin{bmatrix} u_{m,n} \\ v_{m,n} \\ 1 \end{bmatrix} \end{bmatrix} = \begin{bmatrix} \boldsymbol{P}_1 \\ \vdots \\ \boldsymbol{P}_m \end{bmatrix} \begin{bmatrix} \boldsymbol{X}_1 & \cdots & \boldsymbol{X}_n \end{bmatrix} \quad (9)$$

where $\boldsymbol{X}_j = \begin{bmatrix} x_j & y_j & z_j & 1 \end{bmatrix}^T$ (with $j = 1...n$).

Eq. (9) may be rewritten in the following compact form:

$$\boldsymbol{Q} = \boldsymbol{P}\boldsymbol{X} \quad (10)$$

where $\boldsymbol{P} = \begin{bmatrix} \boldsymbol{P}_1 & \cdots & \boldsymbol{P}_m \end{bmatrix}^T$ and $\boldsymbol{X} = \begin{bmatrix} \boldsymbol{X}_1 & \cdots & \boldsymbol{X}_n \end{bmatrix}$.

$\boldsymbol{Q}$ is called the scaled measurement matrix, $\boldsymbol{P}$ and $\boldsymbol{X}$ are respectively referred as the projective motion and the projective shape. If enough noiseless points $\boldsymbol{u}_{i,j} = \begin{bmatrix} u_{i,j} & v_{i,j} & 1 \end{bmatrix}^T$ (with $i = 1...m$ and $j = 1...n$) are collected and all scale parameters λ_i are known, then $\boldsymbol{Q}$ has rank 4 and can be factorized into $\boldsymbol{P}$ and $\boldsymbol{X}$. It should be noted that the only input is the collected set of points $\boldsymbol{u}_{i,j} = \begin{bmatrix} u_{i,j} & v_{i,j} & 1 \end{bmatrix}^T$.

However, scale parameters λ_i are not known in advance. Moreover, some of the points $\boldsymbol{u}_{i,j} = \begin{bmatrix} u_{i,j} & v_{i,j} & 1 \end{bmatrix}^T$ may be missing because of shadowing or simply misdetections. In order to compute the scale parameters λ_i, the missing points are filled in by applying a *rank-4 constraint* [35].

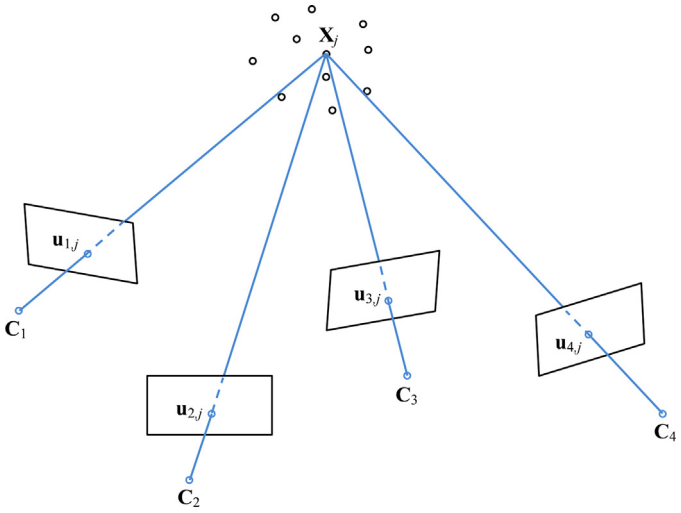

Fig. 3. Schematic illustration of self-calibration of multi-camera system according to the algorithm proposed by Svoboda et al. [10] (C_i is the projection center of camera i, $u_{i,j}$ is the projection point of X_j on the view plane of camera i) [10].

The factorization of Eq. (10) recovers the motion and the shape up to a 4×4 projective transformation $\boldsymbol{H}$:

$$\boldsymbol{Q} = \boldsymbol{PX} = \boldsymbol{PHH}^{-1}\boldsymbol{X} = \hat{\boldsymbol{P}}\hat{\boldsymbol{X}} \tag{11}$$

where $\hat{\boldsymbol{P}} = \boldsymbol{PH}$ and $\hat{\boldsymbol{X}} = \boldsymbol{H}^{-1}\boldsymbol{X}$. Any non-singular 4×4 matrix may be inserted between $\boldsymbol{P}$ and $\boldsymbol{X}$ to get another compatible motion and shape pair $(\hat{\boldsymbol{P}}, \hat{\boldsymbol{X}})$. The self-calibration process computes such a matrix $\boldsymbol{H}$ so that $\hat{\boldsymbol{P}}$ and $\hat{\boldsymbol{X}}$ become Euclidean; in the scientific literature, this process is often called Euclidean stratification [13]. The task of finding the appropriate $\boldsymbol{H}$ can be achieved by imposing specific geometrical constraints. The most general constraint is the assumption that rows and columns of camera chips are orthogonal. Alternatively, it can be assumed that some internal parameters of the cameras are the same, which is more useful for a monocular camera sequence.

The practical implementation of the procedure is based on two steps: (I) reconstruction of the calibration points by using the linear parameters and then (II) feed of these 3D-2D correspondences into a standard method for estimation of the nonlinear distortion and repetition of the self-calibration with the undistorted points. This estimate-and-refine cycle is repeated until the required precision is achieved. This coupled iterative approach typically yields an average re-projection error lower than 1/4 pixel [39].

As a result, the calibration procedure yields, for each camera of the system, the four internal and the six external parameters described above, and the six correction parameters. Whenever camera position and/or orientation are altered, e.g. due to changes in network configuration, a new calibration procedure is required. While every new calibration produces different external parameters, related to the new positions and orientations of cameras, internal and correction parameters remain unchanged unless some functional or structural modifications of cameras occur.

In the scientific literature and in common practice, other calibration procedures are proposed. Special interest has been directed towards the methodology proposed by [46], which involves the use of a calibrated reference artefact, i.e. a planar grid pattern with known geometry, which usually consists of alternating square blocks in black and white including reference markers for plane position and orientation. Even if this approach could produce appreciable results, it has not been included in the present study because it considers each camera individually. The case study reported in this work entails calibration of the whole camera system using a comprehensive method, typically called *multi-camera calibration procedure* [39,22]. Furthermore, the quality and the planarity of the reference pattern have a non-negligible impact on the result of the calibration, so its geometry would need to be accurately calibrated *a priori* [22,3].

4. Multivariate control charts

4.1. General background

The problem of monitoring internal camera parameters can be solved as a process monitoring problem in the Statistical Process Control framework. Univariate control charts could be formulated for each single variable [27], with the drawback, however, of misleading results should variables turn out to be correlated. Furthermore, monitoring of internal camera parameters refers to individual observations, one value only for each parameter being obtained at each calibration. Therefore, specific values of the control limits should be considered for the selected charts. Considering these aspects of using univariate control charts, it is instead preferable to apply multivariate methodologies.

Univariate control of mean and scatter is typically performed using $X-$bar and S control charts [27]. The multivariate extension of $X-bar$ and S control charts are respectively Hotelling T^2 and Generalized Variance control charts [15,28]. These multivariate control charts work well when the number of process variables is not so high, i.e. 10 or less [27,30]]. Furthermore, even if the use of Hotelling T^2 and Generalized Variance control charts is based on the assumption that each of the component variables can be modelled as following a normal distribution, it has been verified that these charts are robust in the presence of significant deviations from this assumption.

In general, the implementation of control charts typically entails two phases. In Phase I, charts are used to test whether the process is *in-control* and collected data are used for the estimation of control limits. In Phase II, charts are used to test whether the process stays *in-control* when subsequent subgroups are drawn using the estimated control limits obtained in Phase I [45].

4.2. Hotelling T^2 control chart

The Hotelling T^2 distance is a measure that accounts for the covariance structure of a multivariate normal distribution [15,30]. It represents the multivariate counterpart of the Student's t statistic.

The formula for computing T^2, for the case of individual observations, is [27]:

$$T_i^2 = \left(\boldsymbol{V}_i - \bar{\boldsymbol{V}}\right)^T \boldsymbol{S}^{-1} \left(\boldsymbol{V}_i - \bar{\boldsymbol{V}}\right) \qquad i = 1, \ldots, k \tag{12}$$

where k is the number of samples used for chart construction in Phase I, $\boldsymbol{V}_i$ is the vector of observations (namely, $\boldsymbol{V}_i = \left[\, u_{0_i} \;\; v_{0_i} \;\; u_{f_i} \;\; v_{f_i} \;\; k_{C1_i} \;\; k_{C2_i} \;\; k_{C3_i} \;\; k_{C4_i} \;\; k_{C5_i} \;\; \alpha_i \,\right]^T$), $\bar{\boldsymbol{V}} = \frac{1}{k} \times \sum_{i=1}^{k} \boldsymbol{V}_i$ is the vector of the corresponding mean values and $\boldsymbol{S}$ is a special estimator of the covariance matrix [14,38], obtained using

$$\boldsymbol{S} = \frac{1}{2 \cdot (k-1)} \boldsymbol{E}^T \boldsymbol{E} \tag{13}$$

where $\boldsymbol{E} = \left[\, \boldsymbol{e}_1^T \;\; \boldsymbol{e}_2^T \;\; \ldots \;\; \boldsymbol{e}_{k-1}^T \,\right]^T$, and $\boldsymbol{e}_1$ are the differences between successive observations:

$$\boldsymbol{e}_l = \boldsymbol{V}_{l+1} - \boldsymbol{V}_l \qquad l = 1, \ldots, k-1 \tag{14}$$

In general, the higher the T^2 value, the more distant is the observation from the mean.

In Phase I, the Hotelling T^2 statistics, in case of individual observations, may be approximated using a Beta distribution with parameters $\frac{p}{2}$ and $\frac{f-p-1}{2}$ [33,40]:

$$T^2 \sim \frac{(k-1)^2}{k} \times \text{Beta}\left(\frac{p}{2}, \frac{f-p-1}{2}\right) \tag{15}$$

with

$$f = \frac{2 \times (k-1)^2}{3 \times k - 4} \tag{16}$$

where p is the number of process variables (namely, in the present case, the number of estimated internal and correction parameters). Therefore, the lower control limit (LCL) and the upper control limit (UCL) are the values of T^2 statistics in Eq. (15) corresponding to a cumulative probability of 0.135% and 99.865%; however, LCL is typically set to zero because any shift in the mean results in an increase in T^2.

It is important to note that the distribution in Eq. (15) is correct only when individual values $\boldsymbol{V}_i$ collected in this Phase are checked to see whether they fall within the control limits. In contrast, in Phase II, when observations are taken and checked against the control limits calculated in Phase I, the statistics that are formed are independent of $\bar{\boldsymbol{V}}$ and $\boldsymbol{S}$ and follow an exact Fisher distribution [41].

By using the special estimator of the covariance matrix $\boldsymbol{S}$ in Eq. (13), the Hotelling T^2 control chart proves to be effective in detecting shifts in the mean vector [14]. The statistical performance of the control chart may be measured through the *Average Run Length* (ARL), which is the expected number of samples taken before a specific shift in the mean vector is detected [27]. Let ARL_d be the ARL of the T^2 chart when the mean vector has shifted from $\bar{\boldsymbol{V}}$ to $\boldsymbol{V}_1$. This shift may be expressed in terms of the Mahalanobis distance d, i.e.

$$d = \sqrt{\left(\boldsymbol{V}_1 - \bar{\boldsymbol{V}}\right)^T \boldsymbol{S}^{-1} \left(\boldsymbol{V}_1 - \bar{\boldsymbol{V}}\right)} \tag{17}$$

It is assumed that the covariance matrix $\boldsymbol{S}$ remains constant when the shift on the mean vector is applied.

The ARL_d can be found by

$$ARL_d = \frac{1}{P_d\left(T_i^2 > UCL \middle| \bar{\boldsymbol{V}} = \boldsymbol{V}_1\right)} \qquad i = 1, \ldots, k \tag{18}$$

where $P_d\left(T_i^2 > UCL \middle| \bar{\mathrm{V}} = \boldsymbol{V}_1\right)$ is the probability that $T_i^2 > UCL$ when the mean vector has shifted from $\bar{\boldsymbol{V}}$ to $\boldsymbol{V}_1$ [23].

The Mahalanobis distance includes in a single value all the possible variations of the averages of the distributions of each of the p parameters; therefore, for a certain value of d, there are an infinite number of combinations of the averages of the distribution of the parameters. Consequently, the ARL_d may only be estimated once the distributions of each of the p parameters are defined.

The use of the Beta distribution in Eq. (15) to approximate the Hotelling T^2 statistics is valid only in Phase I. In contrast, in Phase II, the statistics that are formed are independent of $\bar{\boldsymbol{V}}$ and $\boldsymbol{S}$; hence, it can be demonstrated that the Hotelling T^2 statistics has a Fisher distribution (times a constant) with p and $k-p$ degrees of freedom [41]:

$$T^2 \sim \frac{p \times (k+1) \times (k-1)}{k^2 - k \times p} \times F(p, k-p) \tag{19}$$

Therefore, UCL is now the value of T^2 statistic in Eq. (19) corresponding to a cumulative probability of 99.865% and LCL is, again, set to zero.

4.3. Generalized Variance chart

In general, when data are collected in subsequent samples, the Generalized Variance statistic is $|\boldsymbol{S}|$, i.e. the determinant of the sample covariance matrix [27]. In case of individual observations, all the conventional formulas for the Generalized Variance chart do not work [30]. Therefore, it is necessary to provide an *ad-hoc* procedure [27,26]. All individual observations are standardized by subtracting the relevant column mean and then dividing by the square root of the relevant variance ($S_{j,j}$) taken from the special covariance matrix (see Eq. (13)) [14]:

$$V_i^*(j) = \frac{V_i(j) - \bar{V}_i(j)}{\sqrt{S_{j,j}}} \qquad i = 1, \ldots, k, \qquad j = 1, \ldots, p \tag{20}$$

where $V_i(j)$ and $\bar{V}_i(j)$ are the j-th elements respectively of $\boldsymbol{V}_i$ and $\bar{\boldsymbol{V}}_i$ vectors.

Once the standardized values have been obtained, a traditional S control chart is adopted in which each subgroup corresponds to the components of each $\boldsymbol{V}_i^*$ vector.

The values reported on the Generalized Variance chart, in the case of individual observations, correspond to the standard deviations of the vectors $\boldsymbol{V}_i^*$ components:

$$S_i^* = \sqrt{\frac{\sum_{j=1}^{p}\left(V_i^*(j) - \bar{V}_i^*\right)^2}{p-1}} \qquad i = 1, \ldots, k \tag{21}$$

where $\bar{V}_i^* = \frac{\sum_{j=1}^{p} V_i^*(j)}{p}$ is the mean of the p components of i-th vector.

General Variance control limits are:

$$LCL = \bar{S}^* - 3 \times \frac{\bar{S}^*}{c_4} \times \sqrt{1 - c_4^2} \qquad UCL = \bar{S}^* + 3 \times \frac{\bar{S}^*}{c_4} \times \sqrt{1 - c_4^2} \tag{22}$$

where $\bar{S}^* = \frac{\sum_{i=1}^{k} S_i^*}{k}$ is the average over the k observations of the standard deviations of each vector $\boldsymbol{V}_i^*$ and c_4 is the bias correction of the standard deviation estimate [27]. A central line corresponding to $\bar{S}^*$ is typically shown in the Generalized Variance chart.

For the Generalized Variance charts, the calculation of control limits in Phase I and Phase II is the same.

5. Case study

The previously-described procedure was implemented and tested on a number of different configurations of a commercial multi-camera system Optitrack Flex 13 and some laboratory prototypes at the Quality Engineering Laboratory of DIGEP – Politecnico di Torino, showing good results in terms of reliability and robustness [7,9]. A practical application to a custom-made assembled system is presented below as an example with the aim of highlighting the potentialities of the method.

5.1. Experimental system configuration

The custom-made multi-camera system assembled at DIGEP—Politecnico di Torino was made up of three Hitachi KP-FD140GV RGB color cameras with a resolution of 1280×960 pixel, acquisition rate of 30 frames per second and nominal flange focal distance of 17.5 mm [7,9].

Several camera configurations covering a measuring volume of about $2 \times 2 \times 2\,\text{m}^3$ were calibrated and tested, implementing the procedure on a 40 mm diameter spherical marker.

Table 1
Summary statistics relevant to a set of 30 preliminary calibrations.

	u_0	v_0	u_f	v_f	k_{C1}	k_{C2}	k_{C3}	k_{C4}	k_{C5}	α
Mean	7.03×10^2	5.09×10^2	1.10×10^3	1.10×10^3	-1.23×10^{-1}	2.02×10^{-1}	1.47×10^{-3}	9.83×10^{-4}	-7.33×10^{-5}	1.44×10^{-3}
Standard deviation	7.4×10^0	1.3×10^1	1.1×10^1	1.2×10^1	1.3×10^{-2}	9.2×10^{-2}	1.3×10^{-3}	1.8×10^{-3}	9.6×10^{-5}	1.7×10^{-3}
Variation coefficient	1%	3%	1%	1%	11%	46%	90%	>100%	>100%	>100%

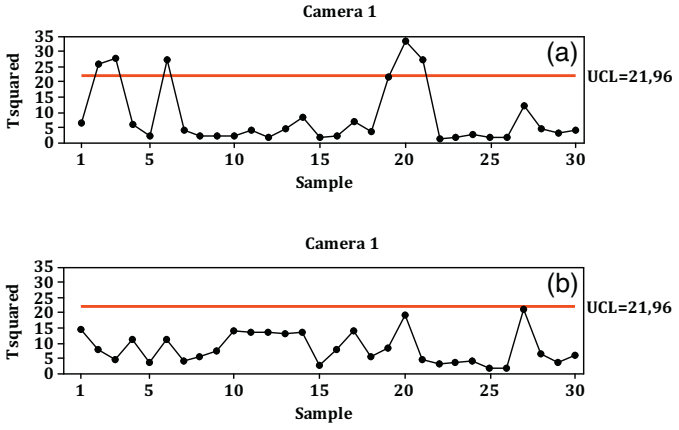

Fig. 4. Hotelling T^2 charts for camera 1: initial (a) and final (b) sets of calibrations, i.e. before and after removing assignable causes of variations.

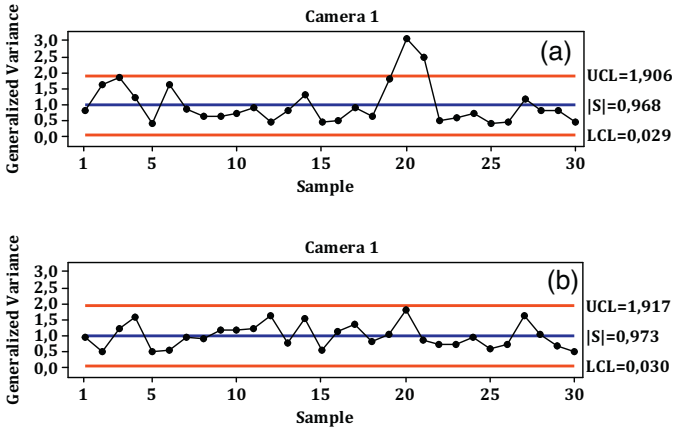

Fig. 5. Generalized Variance charts for camera 1: initial (a) and final (b) sets of calibrations, i.e. before and after removing assignable causes of variations.

A set of 30 preliminary calibrations showed that the parameters k_{C3}, k_{C4}, k_{C5} and α may be considered non-significant. In fact, the corresponding variation coefficients assume values higher than 50%, as shown in Table 1 [27].

Therefore, for each of the three cameras, six parameters only (4 internal and 2 correction) required monitoring.

5.2. Construction of Hotelling T^2 and General Variance control Charts

Multivariate control charts have been used to monitor internal camera parameters and correction parameters of the three-camera system described in the previous Section; therefore, for each camera $p = 6$ parameters have been monitored (namely, u_{0_i}, v_{0_i}, u_{f_i}, v_{f_i}, k_{C1_i} and k_{C2_i}). As mentioned previously, the number of process variables is adequate for the application of Hotelling T^2 and Generalized Variance control charts (see Figs. 4 and 5).

In Phase I, $k = 30$ calibrations were performed to create a historical dataset; this number was chosen based on previous studies that suggested to consider at least twenty calibrations [20], and on time constraints. In order to model *in-control* process performance, further calibrations were performed to remove assignable causes of variation and to substitute *out-of-control* data, as shown e.g. in Figs. 4 and 5.

By way of example, the construction of the multivariate charts represented in Figs. 4(a) and 5(a) is respectively described in Appendix A.1 and A.2. Hotelling T^2 charts control limits, depending only on $p = 6$ variables and $k = 30$ replicates, are unaffected by replacement of data (see Eq. (15)). On the other hand, the limits of the Generalized Variance control charts are liable to vary after replacement of *out-of-control* data, as these limits are directly affected by actual data.

In Phase II, control charts are then used in order to monitor the process.

5.3. Performance evaluation of the applied control charts

The performance of the T^2 control chart has been evaluated by calculating ARL_d for Phase I through simulation for different values of Mahalanobis distance d [23]. It has been assumed that all p parameters have a normal distribution and, given a specific value of d, all their averages vary by the same percentage W (see Eqs. (17) and (18)).

The obtained results are shown in Table 2.

Table 2
ARL_d of the T^2 chart for different values of the Mahalanobis distance d obtained by assuming that all the p parameters have a normal distribution and all their averages vary of the same percentage W.

d	0.75	1	2	3	4	5	6
W	0.45%	0.6%	1.2%	1.8%	2.4%	3.0%	3.6%
ARL_d	386.1	242.3	33.8	6.5	2.2	1.3	1.0

Table 3
ARL_q of the Generalized Variance chart for different values of the amplitude q of the distortion of the distribution of the standard deviation S_i^*.

q	1.0	1.2	1.4	1.6	1.8	2.0
ARL_q	370.4	40.2	9.5	4.2	2.6	1.9

By applying the same procedure for Phase II, similar results are obtained.

Similarly, performance of the Generalized Variance chart has been evaluated through simulation by considering a distortion of amplitude q of the distribution of the standard deviation S_i^*. In particular, it has been assumed that the distorted standard deviation $S_i^{*'}$ has a distribution that can be approximated by a normal distribution with mean $q \cdot \bar{S}^*$ and standard deviation $\frac{q \cdot \bar{S}^*}{c_4} \cdot \sqrt{1-c_4^2}$, with $q \geq 1$. This normal approximation is admissible for a sample size $k = 30$ [17].

It is obtained:

$$\mathrm{ARL}_q = \frac{1}{P_q\left(S_i^{*'} < \mathrm{LCL} \text{ or } S_i^{*'} > \mathrm{UCL} \middle| S_i^{*'} \sim N\left(q \times \bar{S}^*, \left(\left(q \times \bar{S}^*\right)/c_4\right) \times \sqrt{1-c_4^2}\right)\right)} \tag{23}$$

where $P_q\left(S_i^{*'} < LCL \text{ or } S_i^{*'} > UCL \middle| S_i^{*'} \sim N\left(q \times \bar{S}^*, \frac{q \times \bar{S}^*}{c_4} \times \sqrt{1-c_4^2}\right)\right)$ is the probability that $S_i^{*'} < \mathrm{LCL}$ or $S_i^{*'} > \mathrm{UCL}$ when a distortion of amplitude q occurred to the distribution of the standard deviation S_i^*.

By varying the value q, the results shown in Table 3 are obtained.

6. Conclusions

Photogrammetric techniques are widely used in industrial applications of Large-Scale Dimensional Metrology because flexible, low-cost solutions are offered by multi-camera systems. These systems critically rely upon camera calibration, covering estimation of both internal and external parameters. The former require mainly stability, while the latter are affected by camera position and orientation.

Specific procedures and artefacts are usually employed for periodic or systematic calibrations after changes in the spatial configuration of the system. In particular, when photogrammetric systems are used for the regular monitoring on production lines, camera calibration parameters are updated regularly in order to ensure the correct metrological behaviour of the system. Especially for these cases, a diagnostic method for detecting variations of internal parameters is proposed; its main innovative aspect concerns use of multivariate control charts, Hotelling T^2 for mean and Generalized Variance for variability.

This approach, relying only upon data acquired during calibration phase, enables quick and comprehensive stability control at each calibration. Furthermore, it can be easily integrated into calibration software without the need of additional procedures or artefacts.

The robustness and reliability of the method have been proved by tests performed on a commercial multi-camera system and a laboratory prototype assembled at Quality Engineering Laboratory of DIGEP - Politecnico di Torino.

Appendix A.

A.1. Hotelling T^2 control chart application to the proposed case study

The statistics represented in Fig. 4(a) may be obtained through the following procedure. Values $V_i = \left[u_{0_i} \;\; v_{0_i} \;\; u_{f_i} \;\; v_{f_i} \;\; k_{C1_i} \;\; k_{C2_i}\right]^T$ relevant to the initial set of calibrations are shown in Table 4.

The vector of the mean values is $\bar{\boldsymbol{V}} = \left[689.01 \;\; 514.06 \;\; 1091.30 \;\; 1091.07 \;\; -0.12 \;\; 0.20\right]^T$. On the other hand, values $\boldsymbol{e}_1$, i.e. differences between successive observations defined in Eq. (14), are shown in Table 5.

According to Eq. (13), the special covariance matrix is:

$$S = \begin{pmatrix} 9.40 \times 10^{1} & -1.65 \times 10^{1} & -1.86 \times 10^{1} & -1.95 \times 10^{1} & -6.45 \times 10^{-3} & -1.15 \times 10^{-1} \\ -1.65 \times 10^{1} & 2.31 \times 10^{2} & -1.19 \times 10^{1} & -1.16 \times 10^{1} & -1.99 \times 10^{-1} & 4.76 \times 10^{-1} \\ -1.86 \times 10^{1} & -1.19 \times 10^{1} & 1.19 \times 10^{2} & 1.22 \times 10^{2} & -6.07 \times 10^{-2} & 3.67 \times 10^{-1} \\ -1.95 \times 10^{1} & -1.16 \times 10^{1} & 1.22 \times 10^{2} & 1.27 \times 10^{2} & -6.41 \times 10^{-2} & 4.03 \times 10^{-1} \\ -6.45 \times 10^{-3} & -1.99 \times 10^{-1} & -6.07 \times 10^{-2} & -6.41 \times 10^{-2} & 4.83 \times 10^{-4} & -1.35 \times 10^{-3} \\ -1.15 \times 10^{-1} & 4.76 \times 10^{-1} & 3.67 \times 10^{-1} & 4.03 \times 10^{-1} & -1.35 \times 10^{-3} & 8.38 \times 10^{-3} \end{pmatrix}$$

and the corresponding inverse is:

$$S^{-1} = \begin{pmatrix} 1.20 \times 10^{-2} & 2.26 \times 10^{-3} & 3.64 \times 10^{-3} & -1.29 \times 10^{-3} & 2.18 \times 10^{0} & 2.90 \times 10^{-1} \\ 2.26 \times 10^{-3} & 7.71 \times 10^{-3} & 1.16 \times 10^{-3} & 1.62 \times 10^{-3} & 3.74 \times 10^{0} & 6.58 \times 10^{-2} \\ 3.64 \times 10^{-3} & 1.16 \times 10^{-3} & 1.89 \times 10^{0} & -1.85 \times 10^{0} & 1.87 \times 10^{1} & 9.20 \times 10^{0} \\ -1.29 \times 10^{-3} & 1.62 \times 10^{-3} & -1.85 \times 10^{0} & 1.82 \times 10^{0} & -1.68 \times 10^{1} & -9.40 \times 10^{0} \\ 2.18 \times 10^{0} & 3.74 \times 10^{0} & 1.87 \times 10^{1} & -1.68 \times 10^{1} & 5.84 \times 10^{3} & 7.48 \times 10^{2} \\ 2.90 \times 10^{-1} & 6.58 \times 10^{-2} & 9.20 \times 10^{0} & -9.40 \times 10^{0} & 7.48 \times 10^{2} & 2.89 \times 10^{2} \end{pmatrix}$$

According to Eq. (12), the distances reported on the Hotelling T^2 control chart are shown in Table 6.

From Eqs. (15) and (16), since $p = 6$ and $k = 30$, it results $f = 19.56$ and $T^2 \sim 28.03 \cdot \mathrm{Beta}(3, 6.28)$. Therefore, the limit $UCL = 21.96$ shown on the chart is the value of the latter T^2 statistics corresponding to a cumulative probability of 99.865%, while LCL is set to zero. Table 6 shows five calibrations out of control (shown in boldface) over the UCL.

Table 4
Values $\boldsymbol{V}_i$ relevant to the initial set of calibrations.

i	u_{0_i}	v_{0_i}	u_{f_i}	v_{f_i}	k_{C1_i}	k_{C2_i}
1	693.97	514.51	1109.00	1108.64	−0.11	0.17
2	706.67	480.36	1077.95	1074.30	−0.10	0.12
3	691.70	503.33	1104.50	1104.34	−0.15	0.56
4	690.29	510.51	1106.32	1106.07	−0.15	0.35
5	692.92	511.30	1091.80	1092.31	−0.13	0.23
6	674.68	461.70	1096.12	1097.69	−0.11	0.17
7	694.59	499.58	1102.47	1102.59	−0.14	0.24
8	694.41	497.48	1095.30	1095.27	−0.12	0.19
9	688.88	521.38	1082.16	1082.08	−0.11	0.15
10	698.81	501.84	1086.82	1086.30	−0.12	0.15
11	684.62	514.43	1102.35	1102.41	−0.14	0.35
12	683.62	503.96	1092.02	1091.30	−0.11	0.15
13	682.52	521.90	1100.40	1100.30	−0.15	0.18
14	665.50	526.55	1092.55	1092.72	−0.15	0.28
15	693.13	525.79	1092.25	1092.52	−0.13	0.21
16	686.04	514.15	1089.72	1089.85	−0.11	0.12
17	676.77	531.37	1096.12	1096.34	−0.11	0.16
18	688.72	519.59	1101.80	1101.53	−0.12	0.14
19	691.15	497.40	1082.48	1081.42	−0.04	0.11
20	689.77	551.22	1036.64	1035.64	−0.11	0.18
21	670.75	537.87	1059.66	1058.44	−0.06	−0.01
22	691.93	522.50	1087.62	1087.85	−0.13	0.24
23	695.57	526.28	1089.19	1089.17	−0.13	0.20
24	678.82	526.83	1089.21	1089.69	−0.13	0.25
25	696.68	515.99	1095.19	1095.12	−0.12	0.17
26	697.41	511.62	1091.95	1092.10	−0.12	0.16
27	686.84	537.32	1098.15	1096.07	−0.17	0.22
28	705.65	508.23	1089.23	1089.61	−0.13	0.20
29	681.83	506.95	1102.56	1102.47	−0.13	0.21
30	695.94	519.75	1097.41	1098.07	−0.13	0.17

Table 5
Values $\boldsymbol{e}_l$ relevant to the initial set of calibrations.

l	e_{1_l}	e_{2_l}	e_{3_l}	e_{4_l}	e_{5_l}	e_{6_l}
1	12.70	−34.15	−31.05	−34.34	0.01	−0.05
2	−14.97	22.97	26.55	30.04	−0.05	0.44
3	−1.42	7.18	1.82	1.73	0.00	−0.21
4	2.63	0.79	−14.52	−13.76	0.02	−0.11
5	−18.24	−49.59	4.32	5.38	0.02	−0.06
6	19.92	37.87	6.35	4.89	−0.03	0.06
7	−0.19	−2.10	−7.17	−7.32	0.01	−0.05
8	−5.53	23.90	−13.14	−13.19	0.01	−0.04
9	9.94	−19.54	4.66	4.22	0.00	0.00
10	−14.20	12.59	15.53	16.11	−0.02	0.20
11	−1.00	−10.48	−10.33	−11.11	0.02	−0.20
12	−1.10	17.94	8.37	9.00	−0.03	0.04
13	−17.01	4.65	−7.85	−7.58	0.00	0.09
14	27.63	−0.76	−0.30	−0.20	0.01	−0.07
15	−7.09	−11.65	−2.53	−2.67	0.02	−0.09
16	−9.27	17.22	6.41	6.48	0.00	0.04
17	11.95	−11.78	5.67	5.20	−0.01	−0.02
18	2.43	−22.19	−19.32	−20.12	0.07	−0.03
19	−1.38	53.82	−45.84	−45.78	−0.06	0.06
20	−19.02	−13.35	23.02	22.80	0.05	−0.18
21	21.18	−15.38	27.97	29.41	−0.07	0.24
22	3.64	3.78	1.57	1.32	0.00	−0.04
23	−16.74	0.55	0.01	0.52	0.00	0.05
24	17.85	−10.84	5.99	5.44	0.01	−0.09
25	0.73	−4.36	−3.24	−3.02	0.00	−0.01
26	−10.57	25.70	6.20	3.97	−0.04	0.06
27	18.81	−29.09	−8.92	−6.47	0.04	−0.02
28	−23.82	−1.28	13.33	12.87	−0.01	0.01
29	14.11	12.80	−5.14	−4.41	0.01	−0.03

Table 6
Values of T^2 distances relevant to the initial set of calibrations.

i	1	2	3	4	5	6	7	8	9	10	11	12	13	14	15
T_i^2	6.31	**26.52**	**28.06**	5.70	1.73	**27.00**	3.67	2.02	1.71	1.79	3.86	1.39	4.48	8.13	1.56
i	16	17	18	19	20	21	22	23	24	25	26	27	28	29	30
T_i^2	2.06	6.56	3.12	21.64	**33.61**	**27.44**	1.18	1.63	2.50	1.42	1.64	11.42	4.19	3.10	3.72

Table 7
Values $\boldsymbol{V}_i^*$ and S_i^* relevant to the initial set of calibrations.

i	$u_{0_i}^*$	$v_{0_i}^*$	$u_{f_i}^*$	$v_{f_i}^*$	$k_{C1_i}^*$	$k_{C2_i}^*$	S_i^*
1	0.51	0.03	1.62	1.56	0.54	−0.36	0.803
2	1.82	−2.22	−1.22	−1.49	1.14	−0.89	1.593
3	0.28	−0.71	1.21	1.18	−1.25	3.94	1.838
4	0.13	−0.23	1.38	1.33	−1.45	1.61	1.199
5	0.40	−0.18	0.05	0.11	−0.60	0.37	0.375
6	−1.48	−3.44	0.44	0.59	0.52	−0.29	1.593
7	0.58	−0.95	1.02	1.02	−0.66	0.39	0.848
8	0.56	−1.09	0.37	0.37	0.02	−0.11	0.597
9	−0.01	0.48	−0.84	−0.80	0.42	−0.58	0.599
10	1.01	−0.80	−0.41	−0.42	0.29	−0.60	0.680
11	−0.45	0.02	1.01	1.01	−0.61	1.60	0.903
12	−0.56	−0.66	0.07	0.02	0.39	−0.56	0.434
13	−0.67	0.52	0.83	0.82	−1.09	−0.17	0.812
14	−2.42	0.82	0.11	0.15	−1.12	0.83	1.272
15	0.43	0.77	0.09	0.13	−0.46	0.09	0.409
16	−0.31	0.01	−0.15	−0.11	0.63	−0.86	0.482
17	−1.26	1.14	0.44	0.47	0.70	−0.44	0.872
18	−0.03	0.36	0.96	0.93	0.25	−0.64	0.606
19	0.22	−1.10	−0.81	−0.86	3.58	−0.96	1.808
20	0.08	2.44	−5.01	−4.93	0.72	−0.26	**3.094**
21	−1.88	1.57	−2.90	−2.90	2.78	−2.25	**2.468**
22	0.30	0.56	−0.34	−0.29	−0.58	0.41	0.470
23	0.68	0.80	−0.19	−0.17	−0.60	0.00	0.545
24	−1.05	0.84	−0.19	−0.12	−0.37	0.58	0.682
25	0.79	0.13	0.36	0.36	−0.10	−0.35	0.398
26	0.87	−0.16	0.06	0.09	0.02	−0.41	0.430
27	−0.22	1.53	0.63	0.44	−2.00	0.22	1.180
28	1.72	−0.38	−0.19	−0.13	−0.32	−0.05	0.798
29	−0.74	−0.47	1.03	1.01	−0.56	0.06	0.794
30	0.72	0.37	0.56	0.62	−0.23	−0.31	0.448

A.2. Generalized Variance control chart application to the proposed case study

The statistics represented in Fig. 5(a) may be obtained through the following procedure. Values $\boldsymbol{V}_i$ and $\boldsymbol{e}_1$ relevant to the initial set of calibrations are shown in Tables 4 and 5; the vector of the mean values $\bar{\boldsymbol{V}}$ is also reported in the section A.1.

The variance vector, i.e. the diagonal of the covariance matrix S reported in Eq. (13), is $\mathrm{Diag}(\boldsymbol{S}) = \left[9.40 \times 10^1 \;\; 2.31 \times 10^2 \;\; 1.19 \times 10^2 \;\; 1.27 \times 10^2 \;\; 4.83 \times 10^{-4} \;\; 8.38 \times 10^{-3}\right]^T$.

Standardized values $\boldsymbol{V}_i^* = \left[u_{0_i}^* \;\; v_{0_i}^* \;\; u_{f_i}^* \;\; v_{f_i}^* \;\; k_{C1_i}^* \;\; k_{C2_i}^*\right]^T$ defined in Eq. (20) are shown in Table 7 together with the corresponding standard deviations S_i^*.

The average over the $k = 30$ standard deviations S_i^* is $\bar{S}^* = 0.968$ (central line of the Generalized Variance chart), while the value c_4 with $p = 6$ is 0.952. According to Eq. (22), the control limits shown on the chart are LCL = 0.029 and UCL = 1.906.

Since S_{20}^* and S_{21}^* (shown in boldface in Table 7) are greater than *UCL*, the 20th and 21st calibration are out of control and need to be replaced after removing the assignable causes from the process.

References

[1] Aicon official website. Aicon official website; 2014. ⟨http://aicon3d.com/⟩ (accessed October 21st 2014).
[2] Barbato G, Genta G, Germak A, Levi R, Vicario G. Treatment of experimental data with discordant observations: issues in empirical identification of distribution. Meas Sci Rev 2012;12/4:133–40.
[3] Bouguet JY. Camera calibration toolbox for Matlab; 2013. ⟨http://www.vision.caltech.edu/bouguetj/calib_doc/⟩ (accessed 12.12.2013).
[4] Chandler JH, Fryer JG, Jack A. Metric capabilities of low-cost digital cameras for close range surface measurement. Photogramm Rec 2005;20/109:12–26.
[5] Estler WT, Edmundson KL, Peggs GN, Parker DH. Large-scale metrology—an update. CIRP Ann 2002;51/2:587–609.
[6] Fischler M, Bolles R. Random sample consensus: a paradigm for model fitting with applications to image analysis and automated cartography. Commun ACM 1981;24/6:381–95.
[7] Franceschini F, Galetto M, Maisano D, Mastrogiacomo L, Pralio B. Distributed large-scale dimensional metrology. London: Springer; 2011.
[8] Fraser CS. Digital camera self-calibration. ISPRS J Photogramm Remote Sens 1997;52/4:149–59.
[9] Galetto M, Mastrogiacomo L, Pralio B. MScMS-II: an innovative IR-based indoor coordinate measuring system for large-scale metrology applications. Int J Adv Manuf Technol 2011;52/1–4:291–302.
[10] Goch G, Knapp W, Hartig F. Precision engineering for wind energy systems. CIRP Ann 2012;61/2:611–34.
[11] Habib A, Morgan M. Stability analysis and geometric calibration of off-the-shelf digital cameras. Photogramm Eng Remote Sens 2005;71/6:733–41.
[12] Habib A, Pullivelli A, Mitishita E, Ghanma M, Kim E-M. Stability analysis of low-cost digital cameras for aerial mapping using different georeferencing techniques. Photogramm Rec 2006;21/113:29–43.
[13] Hartley RI, Zisserman A. Multiple view geometry in computer vision. Cambridge: Cambridge University Press; 2004.
[14] Holmes DS, Mergen AE. Improving the performance of the T^2 control chart. Qual Eng 1993;5/4:619–25.
[15] Hotelling H. Multivariate quality control. In: Eisenhart C, Hastay MW, Wallis WA, editors. Techniques of statistical analysis. New York, NY: McGraw-Hill; 1947.
[16] JCGM 200. International vocabulary of metrology—basic and general concepts and associated terms (VIM). 3rd ed. Sèvres: JCGM; 2012.
[17] Kenney JF, Keeping ES. The distribution of the standard deviation, §7.8 in mathematics of statistics. 2nd ed. Van Nostram: Princeton; 1951. p. 170–3. Pt. 2.
[18] Läbe T, Förstner W. Geometric stability of low-cost digital consumer cameras. Int Arc Photogramm Remote Sens Spatial Inf Sci 2004;35/B1:528–34.
[19] Lichti DD, Habib A, Detchev I. An object-space simulation method for low-cost digital camera stability testing. Photogramm Eng Remote Sens 2009;75/12:1407–14.
[20] Lowry CA, Montgomery DC. A Review of multivariate control charts. IIE Trans 1995;27/6:800–10.
[21] Lu X, Rao N, Usman I. Six-axis position measurement system for levitated motion stages. CIRP Ann 2013;62/1:507–10.
[22] Luhmann T, Robson S, Kyle S, Harley I. Close range photogrammetry. New York, NY: John Wiley & Sons; 2006.
[23] Mahadik SB. Hotelling's T^2 charts with variable control and warning limits. Int J Qual Eng Technol 2012;3/2:158–67.
[24] Mapvision official website. Mapvision official website; 2014. ⟨http://www.mapvision.fi/⟩ (accessed October 21st 2014).
[25] Mikhail EM, Bethel JS, Mcglone JC. Introduction to modern photogrammetry. New York, NY: John Wiley & Sons; 2001.
[26] Minitab® Statistical Software. Minitab® statistical software, private communication; 2013. October.
[27] Montgomery DC. Introduction to statistical quality control. 6th ed. New York, NY: John Wiley & Sons; 2008.

[28] Montgomery DC, Wadsworth HM. Some techniques for multivariate quality control applications. Trans ASQC 1972;26:427–35.
[29] Muelaner JE, Cai B, Maropoulos PG. Large-volume metrology instrument selection and measurability analysis. Proc Inst Mech Eng, B J Eng Manuf 2010;224/6:853–68.
[30] NIST/SEMATECH. NIST/SEMATECH e-handbook of statistical methods; 2014 January. ⟨http://www.itl.nist.gov/div898/handbook/⟩.
[31] Optitrack official website: https://www.naturalpoint.com/optitrack/.(accessed October 21st 2014).
[32] Peggs GN, Maropoulos PG, Hughes EB, Forbes AB, Robson S, Ziebart M, et al. Recent developments in large-scale dimensional metrology. Proc Inst Mech Eng, B J Eng Manuf 2009;223/6:571–95.
[33] Scholz FW, Tosch TJ. Small sample uni- and multivariate control charts for means. In: 154th Annual Meeting of the American Statistical Society, Quality and Productivity Section. 1994.
[34] Schwenke H, Neuschaefer-Rube U, Pfeifer T, Kunzmann H. Optical methods for dimensional metrology in production engineering. CIRP Ann 2002;51/2:685–99.
[35] Shashua A, Avidan S. The rank 4 constraint in multiple (≥3) view geometry. In: Computer vision—ECCV'96. Cambridge, UK: Springer; 1996. p. 196–206, 14–18 April 1996.
[36] Shortis MR, Bellman CJ, Robson S, Johnston GJ, Johnson GW. Stability of zoom and fixed lenses used with digital SLR cameras. Int Arc Photogramm Remote Sens Spatial Inf Sci 2006;5:289–90, 36/Part.
[37] Stiros SC. Levelling in antiquity: instrumentation, techniques and accuracies. Sur Rev 2012;44/324:45–52.
[38] Sullivan JH, Woodall WH. A comparison of multivariate control charts for individual observations. J Qual Technol 1996;28/4:398–408.
[39] Svoboda T, Martinec D, Pajdla T. A convenient multi-camera self-calibration for virtual environments. Presence: Teleoperators Virtual Environ 2005;14/4:407–22.
[40] Timm NH. Multivariate quality control using finite intersection tests. J Qual Technol 1996;28/2:233–43.
[41] Tracy ND, Young JC, Mason RL. Multivariate control charts for individual observations. J Qual Technol 1992;24/2:88–95.
[42] Vicon official website: https://www.vicon.com.(accessed October 21st 2014).
[43] Wackrow R, Chandler JH, Bryan P. Geometric consistency and stability of consumer-grade digital cameras for accurate spatial measurement. Photogramm Rec 2007;22/118:121–34.
[44] Weckenmann A, Jiang X, Sommer KD, Neuschaefer-Rube U, Seewig J, Shaw L, et al. Multisensor data fusion in dimensional metrology. CIRP Ann 2009;58/2:701–21.
[45] Woodall WH. Controversies and contradictions in statistical process control. J Qual Technol 2000;32/4:341–50.
[46] Zhang Z. A flexible new technique for camera calibration. IEEE Trans Pattern Anal Mach Intell 2000;22/11:1330–4.